Vol. 13: 77–90, 1999 | CLIMATE RESEARCH Clim Res | Published September 7

Radiation balance of wetland tundra at northern treeline estimated from remotely sensed data

Claude R. Duguay[1,*], Wayne R. Rouse[2], Peter M. Lafleur[3], L. Dale Boudreau[2]

[1]Département de géographie et Centre d'études nordiques, Université Laval, Cité Universitaire Sainte-Foy, Quebec G1K 7P4, Canada

[2]School of Geography and Geology, McMaster University, Hamilton, Ontario L8S 4K1, Canada

[3]Department of Geography, Trent University, Peterborough, Ontario K9J 7B8, Canada

ABSTRACT: Traditional methods of measuring surface net radiation involve point measurements that represent only a small area surrounding the instrumented sites. Remotely sensed spaceborne data offer the means by which to obtain estimates of the outgoing fluxes at the regional scale. The objective of this study was to estimate surface albedo, surface thermal exitance, and net radiation using Landsat Thematic Mapper (TM) data over wetland tundra at northern treeline near Churchill, Manitoba, Canada. Ground-based measurements of each component of the radiation balance were acquired at 5 locations coincident with 2 TM overpasses during summer 1991. Each location was representative of 1 of the major terrain types found in the Hudson Bay Lowlands (i.e. sedge-dominated wetland, upland lichen-heath, tundra lakes and ponds, willow/birch wetland, and open spruce-tamarack forest). The mean absolute differences between remote sensing estimates and field measurements (all sites combined) are 0.01 for albedo, 25.7 W m^{-2} for thermal exitance, and 14.1 W m^{-2} for net radiation. The 2 summer 1991 TM images (June and August) were then used to examine within and between terrain type variations in surface net radiation during the growing season. TM imagery from August 1984 and August 1991 were also utilised to investigate differences in surface fluxes between a dry year (1984) and a wet year (1991). Results indicate that surface wetness and, to a lesser extent, phenology are the 2 main factors controlling the radiation balance during the summer period in this subarctic tundra-forest landscape.

KEY WORDS: Radiation balance · Landsat Thematic Mapper · Wetlands · Treeline

1. INTRODUCTION

Accurate quantification of the components of the hydrologic cycle and surface energy balance over a wide range of scales must be accomplished in order to advance our understanding and ability to model land surface and climate interactions. To quantify the hydrologic cycle over subarctic and arctic landscapes, reliable estimates of parameters such as surface net radiation, soil moisture, frozen soil boundaries, vegetation moisture content and snowpack conditions are required. To date, most surface climate studies conducted in northern remote areas have relied on measurements obtained from ground-based instruments. Although field measurement programs provide a good temporal resolution on the daily scale (hourly or half-hourly), the instruments provide a poor spatial representation (on the order of 10 to 100 m^2). In addition, due to the logistics and costs involved in the operation of climate stations in high latitude environments, the measurement programs are often limited to the summer period (June to August). Satellite remote sensing offers a potential means of estimating surface climate variables over large heterogeneous areas with the spatial (e.g. 10 m to 8 km) and temporal resolutions (e.g. half-hour to a few weeks) required for many climate related investigations. Since the temporal resolution of satellites is, in general, inversely related to their spatial resolution, much can be learned from the combination

*E-mail: claude.duguay@ggr.ulaval.ca

of satellite imagery and surface-based measurements (Lafleur et al. 1997). The present study focuses on the use of Landsat Thematic Mapper (TM) imagery (30 m × 30 m pixels) which is best suited for examining spatial variations in surface net radiation on a seasonal time scale.

Recently, new approaches have been proposed to estimate components of the radiation and energy balance using ground-based and airborne and satellite remotely sensed data over diverse landscapes. These approaches have proven to be very successful for obtaining local- and regional-scale estimates over relatively homogeneous land surfaces (e.g. bare soil and agricultural crops) (Daughtry et al. 1990, Kustas et al. 1990). However, serious difficulties have been encountered when applied to surfaces with incomplete vegetation cover (e.g. semiarid rangeland) (Humes et al. 1994, Moran et al. 1994, Kustas et al. 1994a). In order to improve upon current approaches and make them truly operational, there is a need to conduct large-scale experiments over a wide range of landscapes (e.g. boreal forest, subarctic and arctic tundra).

In this paper, we describe an experiment conducted using Landsat TM data to estimate the radiation balance of wetland tundra at northern treeline near Churchill, Manitoba, Canada. Remotely sensed estimates of net radiation and its surface components, namely surface albedo and thermal exitance, are compared with field measurements acquired on 2 Landsat overpass dates over the 5 major terrain types found in this area (i.e. sedge-dominated wetland, upland lichen-heath, tundra lakes and ponds, willow/birch wetland, and open spruce-tamarack forest). Sources of errors in the remote sensing estimates as well as those related to the ground-based measurements are discussed. The spatial variability of the surface fluxes is then examined through the analysis of Landsat TM images acquired in August 1984 as well as June and August 1991.

2. STUDY AREA AND DATA COLLECTION

2.1. Study area. The study area is located in the Hudson Bay Lowlands near Churchill, Manitoba. This area

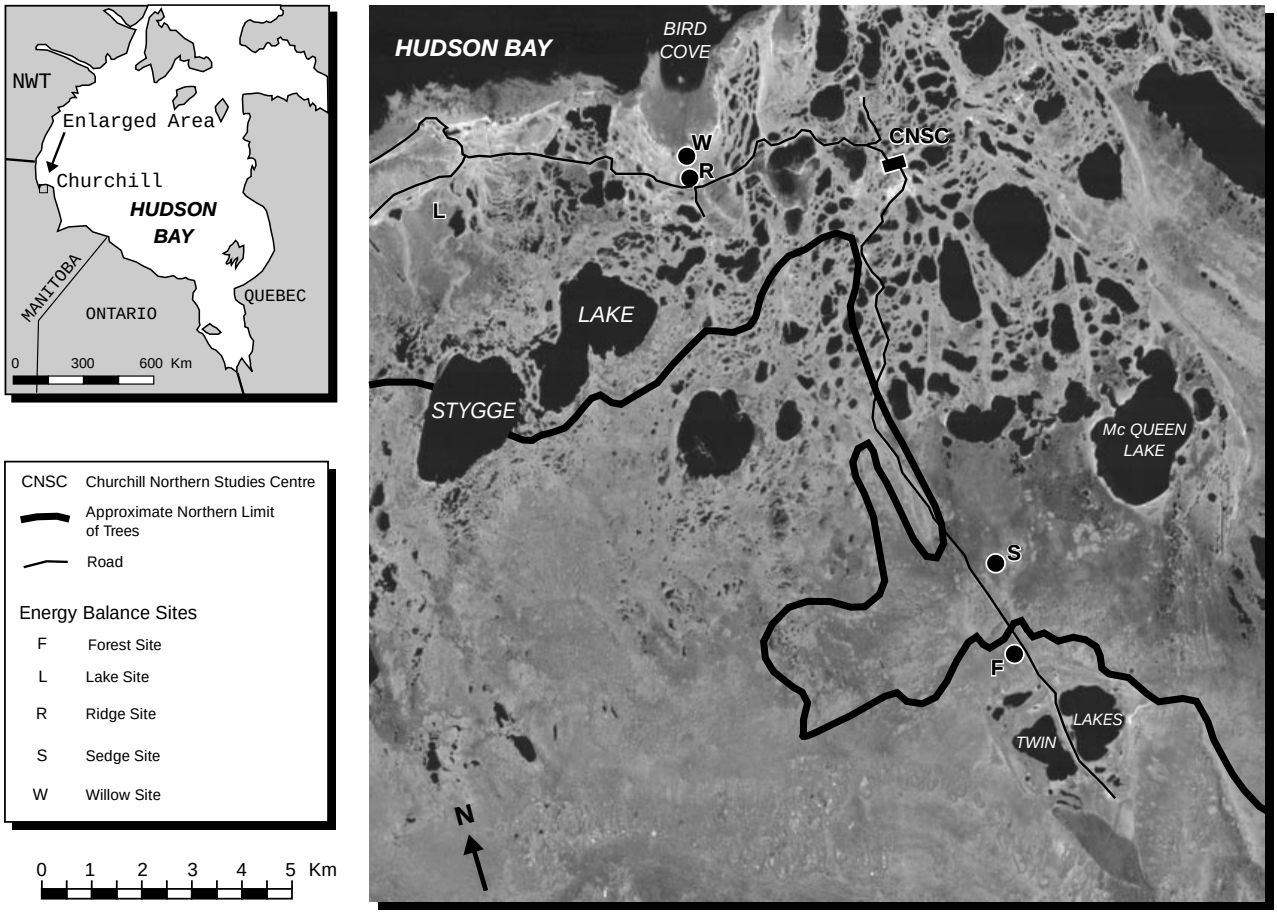

Fig. 1. Location of study area and field measurement sites

(18 km × 18 km) extends south from Hudson Bay toward the Twin Lakes Ecological Reserve (Fig. 1). The regional terrain is generally flat, with glacial deposits forming the major relief in the area. Many small, shallow lakes and ponds occupy between 10 and 30% of the area. Marine silt/clays underlie all the soils in the region. The raised features (raised beaches) generally have poorly developed soils with a very thin (<20 mm) organic soil. Peat topsoil dominates the low-lying areas, and ranges from 100 to 500 mm thick. Permafrost is widespread in the region, and maximum summer active layer depths vary with climate and terrain type, but typically average about 0.7 to 1.0 m. Permafrost terrain features such as patterned ground and palsas are common in the area. Mean annual temperature is –7.2°C, with July temperatures averaging around 12.0°C. Total annual precipitation is 411 mm, of which 235 mm falls as rain during the months of May to September. Snow usually covers the landscape from October to May.

The Churchill area was selected in this study principally for 3 reasons. First, to our knowledge, no previous research has been conducted to map the regional radiation balance over subarctic or arctic land surfaces using remotely sensed data. Second, except for the experimental sites selected for international research initiatives (e.g. FIFE, BOREAS, and GEWEX), the number of instrumented stations that simultaneously measure the fluxes at the satellite passage, over a given research site, is often limited to 1 or 2. In the present research, measurements were acquired simultaneously over 5 different terrain types for 2 Landsat overflight dates. Third, the Churchill study area is one of the best instrumented northernmost sites in Canada. Microclimate studies have been conducted in the area since the late 1970s (Rouse 1984). The longest running program has been the continuous measurements of radiation, energy and water budgets at 2 sites (wet sedge tundra and open forest) for 10 summers (1989–1998).

2.2. Remotely sensed data and ground-based measurements. Three Landsat TM images were acquired under clear sky conditions on 2 August 1984, 28 June 1991, and 6 August 1991, near 10:30 h local solar time. Simultaneous field measurements of incoming solar radiation, surface albedo, surface temperature and net radiation were obtained at 5 sites representative of the major terrain types found in the study area on 28 June and 6 August 1991 (Table 1). No radiation measurements were made during summer 1984. Atmospheric emittance was derived as a residual of the radiation balance equation. Measurements were taken 18.0 m above ground at the forest site and at a height of 2.5 m at the other sites. Maximum relative errors of the field measurements are estimated at ±10% for Q^*, ±5% for $K\downarrow$ and $K\uparrow$, and ±1% for T_s. Given the typical errors in Q^*, $K\downarrow$, $K\uparrow$, and T_s, the root mean square error for $L\downarrow$ is in the order of ±13%.

Table 1. Terrain characteristics of the instrumented sites shown in Fig. 1

Site	Terrain characteristics
Forest	The dominant tree species consist of spruce *Picea mariana* and tamarack *Larix laricina*. The forest floor is a complex arrangement of hummocks and hollows covered with lichen and heath species along with herbaceous plants and small shrubs. Mean tree height is 5.5 m, mean distance between trees is 3 m, and leaf area index is estimated at 1.6
Sedge	Hummocky terrain with *Carex aquatilis* as the dominant species. The water table is generally at or near the surface in the hollows. The hummock tops are covered with communities of lichens and some vascular plants
Lake	North-south oriented lake with an area of roughly 19.2 ha and mean depth of 878 mm. The lake bed is a mixture of decomposing organic ooze and calcareous material about 300 mm thick overlying clay/silt
Ridge	Raised beach ridge with poorly developed soil which supports xerophytic plants, particularly lichen and heath species. The dominant lichen species are *Cladina stellaris* and *C. rangiferina*
Willow	Confined to a band of vegetation immediately adjacent to the coast. The forest consists of willows *Salix candida, S. planifolia* and *S. reticulata* and birches *Betula glandulosa* with a mean height of 0.43 m

The image data set permitted us to: (1) evaluate the difference between Landsat-derived estimates of the surface components of the radiation balance with ground-based measurements (summer 1991), (2) examine the spatial variability of surface net radiation within and between sites during the growing season (June vs August 1991), and (3) examine the effect of surface wetness (dry year of 1984 vs wet year of 1991) on the spatial variability of net radiation within and between sites.

As shown in Fig. 2, summer 1991 was atypical of the 'normal' conditions that have been observed in the area over the last 50 yr with respect to both temperature and precipitation (Boudreau & Rouse 1995). Average temperatures for the months of June, July, and August 1991 were more than 3°C above normal. The amount of rainfall in July and mean air temperature in August were the highest and second highest, respectively, ever recorded at the Churchill Airport climate station. Because of the shallow nature of the unfrozen ground above permafrost in the study area, larger amounts of rainfall and milder temperature conditions in summer can substantially increase the soil moisture

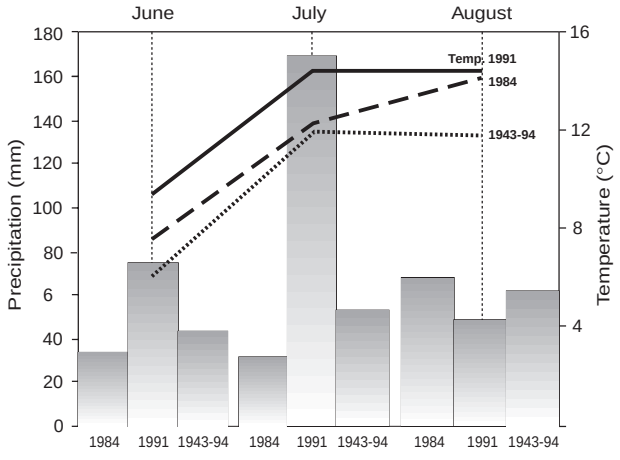

Fig. 2. Summer temperature and precipitation regimes for 1984, 1991, and 1943–1994 means. Landsat TM images acquired in 1984 and 1991 correspond to a relatively dry and very wet summer, respectively, in comparison to mean conditions

level. Mean temperatures during summer 1984 were also above normal but with precipitations below normal, hence resulting in relatively dry surface conditions.

3. ESTIMATION OF THE RADIATION BALANCE

Net radiation is typically the largest term in the energy balance equation, and represents the amount of energy available for partitioning into ground heat flux and sensible and latent heat exchange with the atmosphere. The surface radiation balance is given as

$$Q^* = K\downarrow (1 - \alpha) + L\downarrow - L\uparrow \quad (1)$$

where Q^* is the net allwave radiation, $K\downarrow$ is the incoming solar flux, α is surface albedo ($K\uparrow/K\downarrow$), and $L\downarrow$ and $L\uparrow$ are the atmospheric and terrestrial emitted longwave fluxes.

The approach employed in this analysis is based on previous work by Duguay (1994, 1995) on the radiation balance of alpine tundra surfaces. In this approach, the LOWTRAN 7 radiative transfer code is used to calculate incoming solar radiation for the spectral ranges covered by the Landsat TM bands (Table 2) and to correct for atmospheric effects due to path radiance and atmospheric transmittance in the short- and longwave portions of the electromagnetic spectrum. For this study, 24, 28, and 20 visibility subarctic summer atmospheres were specified in LOWTRAN to represent atmospheric conditions observed on 2 August 1984, 28 June 1991 and 6 August 1991, respectively. Computed incoming short- and longwave radiation fluxes within the bandpass of the field instruments were assumed to be constant over the area of interest (18 km × 18 km), the terrain being relatively flat. Surface albedo and thermal exitance values were then estimated remotely following the approach presented by Duguay & LeDrew (1991, 1992) and Duguay (1994, 1995), and summarised below.

3.1. Surface albedo. An estimation of surface albedo from remotely sensed reflectance measurements can be obtained when the following 3 factors are considered (Brest 1987, Duguay & LeDrew 1992): (1) the spectral reflectance of the surface of interest; (2) the spectral distribution of the irradiance; and (3) the wavelength region of the discrete spectral bands. In this approach, the spectral reflectance curve of the material being sensed is divided into segments of uniform reflectance. Each segment of the curve can then be represented by a band measurement located within the range of the segment. In this approach, land covers are first classified into 3 broad categories: vegetated (forest and alpine tundra), non-vegetated (water, bare soil, rock, etc.), and snow-covered surfaces. A weighting scheme is then assigned to a particular category based on the spectral reflectance curve characterising it (see Duguay & LeDrew 1992 for details). This approach has been used successfully over urbanised areas using Landsat MSS (e.g. Brest 1987) as well as alpine tundra vegetation (Duguay & LeDrew 1991, 1992) and snowfields and glaciers (Crevier & Duguay 1993, Duguay 1993, Koelemeijer et al. 1993, Knap 1997) with Landsat TM.

Two implicit assumptions in this method are that the sensor views the surface from nadir and that the ground cover is lambertian (i.e. near-nadir reflectance is equal to hemispherical reflectance). Given these assumptions, surface reflectance for each TM band (ρ) is given by

$$\rho = \pi (L^* - L_p)/(\tau_v E) \quad (2)$$

where L^* is the apparent radiance at the sensor (W m^{-2} sr^{-1} µm^{-1}), L_p is the path radiance between the satellite

Table 2. Sensor characteristics and exo-atmospheric solar irradiances for Landsat-5 TM. Spatial resolution: 30 m (Bands 1–5, 7) and 120 m (Band 6)

TM band	Spectral coverage (µm)	Centre wavelength (µm)	Exo-atmospheric solar irradiance (W m^{-2} µm^{-1})
1	0.45–0.52	0.4863	1959.20
2	0.52–0.60	0.5706	1827.40
3	0.63–0.69	0.6607	1550.00
4	0.76–0.90	0.8382	1040.80
5	1.55–1.75	1.677	220.75
6	10.40–12.50	11.052	Thermal band
7	2.08–2.35	2.223	74.96

sensor and the surface (W m^{-2} sr^{-1} μm^{-1}), τ_v is the vertical transmission from the surface to the sensor (unitless), and E is the downwelling spectral irradiance at the surface (W m^{-2} μm^{-1}).

Apparent radiances at the sensor were obtained with the following equation:

$$L^* = (DSL - DSL_0)/G \quad (3)$$

where DSL is the digital signal level (or digital count), and G and DSL_0 are the radiometric calibration gain and offset coefficients, respectively. Gain and offset coefficients used in this study were taken from Teillet & Fedosejevs (1995).

Surface albedos were then computed from the satellite derived reflectances for each band according to the method developed by Duguay & LeDrew (1992) for TM imagery. Land surface types found in the 2 TM images were classified, using a simple band ratio (TM 4/TM 2), as vegetated or non-vegetated (e.g. water, roads, etc.). A somewhat subjective threshold of 1.0 was chosen, where pixels with values <1.0 were assumed to be non-vegetated and pixels with values ≥1.0 vegetated. For vegetated surfaces, the following equation is used:

$$\alpha = 0.526\rho_{TM2} + 0.362\rho_{TM4} + 0.112\rho_{TM7} \quad (4)$$

Finally, for non-vegetated surfaces, albedos are computed as follows

$$\alpha = 0.526\rho_{TM2} + 0.474\rho_{TM4} \quad (5)$$

3.2. Surface thermal exitance. The total spectral radiance reaching a sensor in the thermal infrared can be expressed as (Schott & Volchok 1985, Bartolucci et al. 1988)

$$L[\lambda,z] = \varepsilon_s L_T[\lambda]\tau_v[\lambda,z] + \rho L_D[\lambda,z]\tau_v[\lambda,z] + L_U[\lambda,z] \quad (6)$$

where $L[\lambda,z]$ is the total spectral radiance reaching the sensor at altitude z, ε_s is the emissivity of the surface observed, $L_T[\lambda]$ is the blackbody radiance associated with an object on the ground with temperature T, $\tau_v[\lambda,z]$ is the spectral vertical transmission to altitude z, ρ is the reflectance of the surface observed ($\rho = 1 - \varepsilon_s$) in the thermal portion of the electromagnetic spectrum, $L_D[\lambda,z]$ is the downwelled spectral atmospheric radiance, and $L_U[\lambda,z]$ is the upwelled spectral atmospheric radiance (i.e. path radiance). Atmospheric effects (i.e. path radiance and vertical transmission) can be calculated using a radiative transfer code such as LOWTRAN (e.g. Pierce & Congalton 1988, Wukelic et al. 1989) or corrected empirically using surface reference targets such as water bodies (e.g. Lathrop & Lillesand 1987).

The empirically based approach was adopted in the present study for the following 2 reasons: (1) surface temperature measurements using thermocouples were acquired coincident with the TM overpass and (2) clear sky conditions prevailed across the study area at the time of image acquisition. Results of investigations by Lathrop & Lillesand (1987), Bartolucci et al. (1988), Wukelic et al. (1989), and Duguay (1993) have shown that, on relatively clear days, uncorrected TM Band 6 data give a good approximation of ground truth temperatures, and that lakes are the most suitable calibration targets. According to Bartolucci et al. (1988), the atmospherically attenuated target radiance appears to be compensated by the path radiance under clear conditions.

Surface brightness temperature measurements are derived from Landsat TM thermal Band 6 using the equation (Schott & Volchok 1985):

$$T_s = K_2/[\ln(K_1/L[\lambda] + 1)] \quad (7)$$

where K_1 is the first constant (60.776 mW cm^{-2} sr^{-1} μm^{-1}), K_2 is the second constant (1260.56 K), and $L[\lambda]$ is the spectral radiance reaching the sensor (mW cm^{-2} sr^{-1} μm^{-1}).

Under clear sky conditions, surface thermal exitance can then be determined using the Stefan-Boltzman relationship

$$L\uparrow = \varepsilon_s \sigma T_s^4 \quad (8)$$

In the present study, a constant emissivity value of $\varepsilon_s = 0.98$ was assigned to each of the 5 main terrain types found in the area of interest.

4. RESULTS

4.1. Comparison of Landsat-5 TM estimates with ground-based measurements

The comparison of the radiation balance and its surface components measured at each site to the fluxes estimated with Landsat TM is shown in Table 3. For each data point the instantaneous estimate of the flux using Landsat data is compared with the flux measured at the ground-based station. The flux measurement from each station used for comparison is the one corresponding to the 30 min time period which includes the time of the Landsat TM overpasses (28 June and 6 August 1991). The results for the reflected shortwave radiation, thermal exitance, and net radiation are shown graphically in Fig. 3. The root-mean-square errors (RMSE) and mean absolute differences (MAD) between the ground-based measurements and Landsat TM estimates are given on each plot, together with a 1:1 line. This line represents the exact agreement between the estimated fluxes and the measured fluxes.

Surface reflected shortwave radiation ($K\uparrow$) estimates are generally in good agreement with field measurements, differences varying between 0.10 and 14.80 W

Table 3. Comparison of Landsat TM estimates and ground-based measurements (italic) of the components of the radiation balance for 5 terrain types on (a) 28 June and (b) 6 August 1991. The Landsat-derived values correspond to the mean calculated from a 3 × 3 window centred on the measurement stations. $K\downarrow$ and $K\uparrow$: incoming and surface reflected solar flux; α: surface albedo ($K\uparrow/K\downarrow$); $L\downarrow$ and $L\uparrow$: atmospheric and terrestrial emitted longwave fluxes; ε_s: emissivity of the surface observed; Q^*: net allwave radiation

Site	α	$K\uparrow$ (W m^{-2})	$L\uparrow$ (ε_s = 0.98) (W m^{-2})	Q^* (W m^{-2})
(a) 28 June 1991 ($K\downarrow$ = 785.0 W m^{-2}; $L\downarrow$ = 256.5 W m^{-2})				
Forest	0.11	86.4	401.5	553.7
	0.12	*92.3*	*357.0*	*569.0*
Sedge	0.09	70.7	409.2	561.7
	0.09	*67.7*	*370.1*	*564.8*
Lake	0.05	39.3	361.7	640.6
	0.03	*25.1*	*354.2*	*655.2*
Ridge	0.13	102.1	426.8	512.7
	0.14	*111.0*	*395.5*	*535.0*
Willow	0.13	102.1	399.3	540.2
	0.13	*102.0*	*352.0*	*550.2*
(b) 6 August 1991 ($K\downarrow$ = 685.6 W m^{-2}; $L\downarrow$ = 291.3 W m^{-2})				
Forest	0.12	82.3	438.7	453.7
	0.12	*81.6*	*419.6*	*471.0*
Sedge	0.08	54.9	418.8	503.5
	0.08	*54.8*	*430.5*	*505.4*
Lake	0.05	34.3	386.2	553.8
	0.04	*26.4*	*387.7*	*586.2*
Ridge	0.13	89.1	433.2	457.8
	0.15	*103.9*	*455.2*	*443.4*
Willow	0.15	102.8	420.0	456.9
	0.16	*110.8*	*386.7*	*466.3*

m^{-2} (or 0.00 and 0.02 in terms of albedo [α]) depending upon terrain type. When all 5 sites are lumped together, the RMSE is 8.2 W m^{-2} and MAD is 6.4 W m^{-2} (or 0.01 with respect to α). The best results are obtained at the sedge site, followed by the forest and willow sites. With the exception of the lake site, the Landsat-derived values are generally less than those measured in the field. This can be attributed, at least in part, to the instrumentation set up (location and height of instruments above ground). At the lake site, the differences can be explained by the non-lambertian (specular) nature of water. Although the forest site, for example, shows a higher degree of complexity (terrain variability) at the microscale, measurements at the tower (18 m) and those estimated with TM indicate that this surface acts as a lambertian reflector when observed at a smaller scale (i.e. coarser spatial resolution). Observations of the daily variations of α at the forest site on the 2 Landsat overpass dates substantiates this argument (Fig. 4). The hourly and daily average α values were 0.12 on both overpass dates.

Table 3 also shows an excellent agreement between remotely sensed and ground-based thermal exitance ($L\uparrow$) values for the lake site, but differences of up to about 48 W m^{-2} are observed at the other sites. The main reason explaining the large discrepancies for most surfaces is that measurements acquired in the field were contact (kinetic) temperature measurements (ca 2.5 cm below the surface), while the Landsat TM estimates are based on the measurement of brightness (non-contact) temperatures. In addition, the spatial resolution of TM Band 6 is 120 m and thus represents the integration of a signal over a much larger area than the field instruments. Thus, the range in differences between the remote sensing and ground-based observations on a given date can be explained in terms of surface complexity. Two factors play a role in this behaviour: the vegetation canopy and wetness. Complex vegetation shades the soil surface, decoupling the contact and brightness temperature somewhat, as is evidenced for the willow and forest sites. For the sparsely vegetated sites, wetness controls the coupling of contact and brightness temperatures. A dry surface, like that found at the ridge site, produces large thermal gradient in the upper soil layers, again decoupling the 2 estimates of surface temperature. The sedge site which is moderately wet and has a simple canopy gives the closest coupling between brightness and contact temperatures. When looking at the June data alone (Table 3a), the ground-based measurements are much lower than those estimated with Landsat TM (difference of 31 to 47 W m^{-2} when the lake site is excluded). Differences of this magnitude are expected as the frost table is typically located 15 to 40 cm (depending on terrain type) below the surface in late June (Boudreau & Rouse 1995).

Net radiation (Q^*) estimates are also in good agreement with the observed values at all sites, with a mean absolute difference of 14.1 W m^{-2}; well within the ±10% instrument error. The best Q^* estimates are obtained at the sedge fen site with a mean difference of less than 3 W m^{-2}, followed by the willow, forest, ridge, and lake sites. The larger differences in Q^* at the ridge site and particularly the lake site can be attributed, at least in part, to Landsat TM α estimates being lower than those observed in the field on both overpass dates.

4.2. Spatial and temporal variability of surface fluxes

Maps of α, $L\uparrow$, and Q^* on 6 August 1991 (near 10:30 h solar time, at the time of Landsat overflight) (Fig. 5) are shown as an illustration of products derived from the approach described earlier. Test sites for each of the 5 terrain types were identified for analysis. Means and standard deviations for the test sites from the 1991 and 1984 images are compared in Table 4.

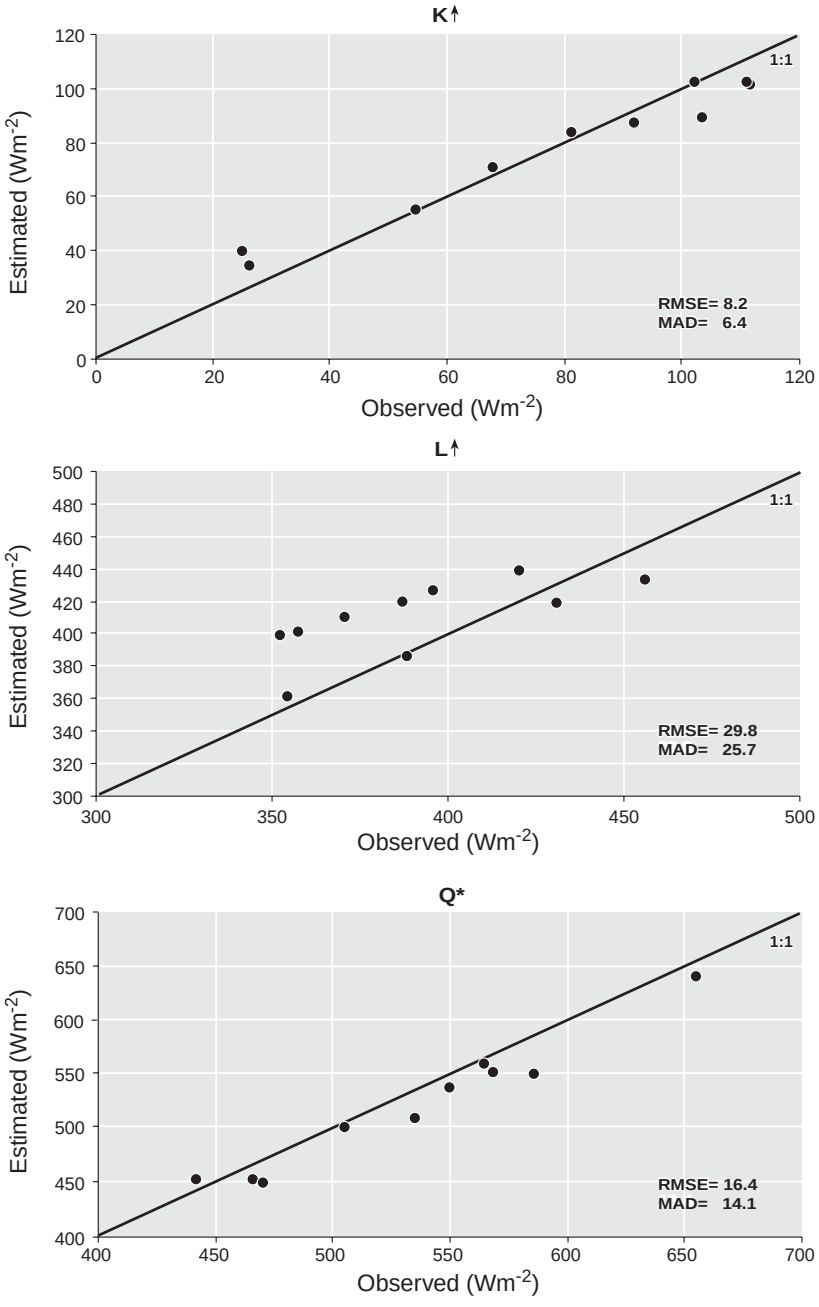

Fig. 3. Comparison between estimated and observed values of surface reflected solar radiation ($K\uparrow$), thermal exitance ($L\uparrow$), and net radiation (Q^*). Observed values from the 5 measurement sites were obtained coincident with Landsat-5 TM overpasses of 28 June and 6 August 1991. Both the root-mean-square error (RMSE) and mean absolute difference (MAD) are given in units W m^{-2}

4.2.1. 1991 growing season

A comparison of the mean fluxes for 28 June and 6 August 1991 suggests that there are primarily 2 controls on the temporal variations during the growing season: phenology and surface wetness. The increase in α observed at the willow site from late June to early August is due to an increase in leaf area index (LAI). Blanken & Rouse (1994) have shown that the development of leaves during the growth period increases α from 0.12 to 0.17 (Fig. 6). The decrease of 0.01 in α between the 2 Landsat acquisitions at the ridge and sedge sites are due to the abnormally large amount of rain that fell in the month of July, thus resulting in wetter surface conditions. At the forest site α remained at a constant value of 0.12. Although changes in water table at this site can be as large as the sedge site, the extent of open water is less and the forest canopy and understorey mask the effects of wetness changes on α (Lafleur et al. 1997). Table 4 also shows that within terrain type variations in α are small on both dates (0.00 to 0.01), regardless of variations in surface wetness and phenological changes. Between terrain type variations, however, are larger, with values varying from 0.05 (lake site) to 0.15–0.16 (willow site).

Within terrain type variability in $L\uparrow$ observed by Landsat TM is also small at all sites on both dates (2.4 to 10.3 W m^{-2} or 1 to 2 K). This may be a result of the 120 m pixel size for brightness temperature masking much of the large variability found at the microscale, say between hummocks and hollows. The variations within terrain types are slightly larger on the June than on the August acquisition date. As shown earlier for α, both surface moisture conditions and phenology can explain most of the differences in $L\uparrow$. The larger standard deviation calculated in late June at the willow site, for example, can be attributed to a greater contribution from the ground, as opposed to the August acquisition date when leaves reach maturity (LAI of about 0.2 in late June and 0.75 in early August 1991) (Blanken & Rouse 1994). At the sedge site, on the other hand, a combination of both moisture (e.g. percent standing water) and phenology provides an explanation for differences between the 2 dates. Between terrain type differences on a given date, however, are larger (range of 55.3 W m^{-2} in June and 45.8 W m^{-2} in

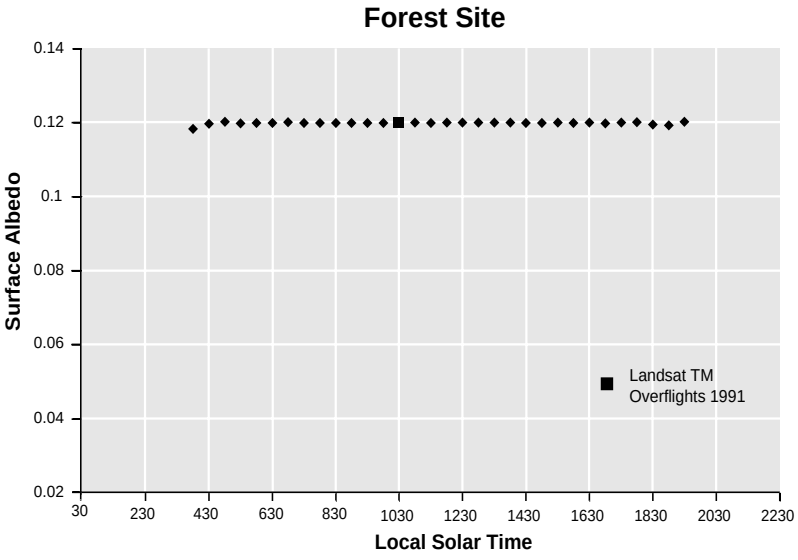

Fig. 4. Daily variations in surface albedo at the forest site on 28 June and 6 August 1991

August). When the lake site is excluded, differences are on the order of 14 W m^{-2} (August) to 19 W m^{-2} (June). Since the Landsat TM data are acquired near 10:30 h local solar time, larger $L\uparrow$ values are observed at the dryer ridge site, followed by the willow, forest, sedge, and lake sites.

Spatial variation in Q^* within the terrain types is generally larger than for the components of the balance (e.g. α and $L\uparrow$). As expected, variation in Q^* increases with surface cover complexity on both dates (e.g. 4 to 6 W m^{-2} for lake and ridge sites and 8 to 17 W m^{-2} for forest, willow and sedge sites). Spatial variation between terrain types (37.9 to 45.7 W m^{-2} without lake site and 110.5 to 126.9 W m^{-2} with lake site) is considerably larger than within terrain types, suggesting that the methodology is a reasonable approach for determining areal estimates of Q^*. We examined the effects of pixel aggregation on such areal estimates on 6 August 1991 (Fig. 7). In this simple experiment, the value of each 120 m pixel is calculated as the average of a 4×4 block of 30 m pixels, that of a 240 m pixel by an 8×8 block, and so on. Decreasing the spatial resolution from the original 30 m TM pixel to a 960 m pixel (approximately equivalent to the AVHRR 1.1 km pixel resolution) gives no change in the mean Q^* for the scene (490.54 W m^{-2} at 30 m compared to 491.17 W m^{-2} at 960 m). However, at the coarser resolution of AVHRR many of the small lakes in the northern sector of the scene are not represented.

4.3.2. Dry year (1984) versus wet year (1991)

The comparison of Landsat estimates from 6 August 1991 and 2 August 1984 reveals that dryer conditions result in higher α values at all terrestrial sites. An increase of 0.02 is noted at the sedge and ridge sites and a smaller increase of 0.01 is observed at the forest and willow sites. As indi-

Table 4. Landsat TM mean (standard deviation) estimates of the components of the radiation balance for 5 terrain types on (a) 28 June 1991, (b) 6 August 1991 and (c) 2 August 1984. n is the number of pixels extracted over a large area which encompasses the measurement stations. For definitions, see Table 3 legend

Site	α	$K\uparrow$ (W m^{-2})	$L\uparrow$ (ε_s = 0.98) (W m^{-2})	Q^* (W m^{-2})
(a) 28 June 1991 ($K\downarrow$ = 785.0 W m^{-2}; $L\downarrow$ = 256.5 W m^{-2})				
Forest (n = 365)	0.12 (0.01)	93.0 (5.9)	404.5 (5.6)	544.0 (8.8)
Sedge (n = 1037)	0.11 (0.01)	83.6 (10.9)	410.7 (8.2)	547.2 (14.4)
Lake (n = 32)	0.05 (0.00)	37.2 (1.7)	368.2 (3.7)	636.2 (4.5)
Ridge (n = 85)	0.13 (0.00)	103.9 (3.0)	423.5 (2.4)	514.1 (4.3)
Willow (n = 175)	0.15 (0.01)	120.2 (8.8)	412.0 (10.3)	509.3 (17.0)
Mean	0.11	87.6	403.8	550.2
Minimum	0.05	37.2	368.2	509.3
Maximum	0.15	120.2	423.5	636.2
Range	0.10	83.0	55.3	126.9
(b) 6 August 1991 ($K\downarrow$ = 685.6 W m^{-2}; $L\downarrow$ = 291.3 W m^{-2})				
Forest (n = 365)	0.12 (0.01)	84.9 (4.7)	423.9 (5.2)	468.1 (7.9)
Sedge (n = 1037)	0.10 (0.01)	65.9 (7.5)	422.0 (3.4)	489.9 (11.0)
Lake (n = 32)	0.05 (0.00)	32.1 (1.4)	390.1 (5.9)	554.7 (5.7)
Ridge (n = 85)	0.12 (0.01)	84.9 (3.6)	435.9 (4.0)	456.0 (6.4)
Willow (n = 175)	0.16 (0.01)	106.6 (6.8)	426.1 (7.0)	444.2 (10.1)
Mean	0.11	74.8	419.6	482.6
Minimum	0.05	32.1	390.1	444.2
Maximum	0.16	106.6	435.9	554.7
Range	0.11	74.5	45.8	110.5
(c) 2 August 1984 ($K\downarrow$ = 734.0 W m^{-2}; $L\downarrow$ = 268.9 W m^{-2})				
Forest (n = 365)	0.13 (0.01)	94.7 (5.7)	416.1 (2.8)	492.2 (7.1)
Sedge (n = 1037)	0.12 (0.01)	89.7 (6.7)	451.3 (5.4)	461.9 (6.4)
Lake (n = 32)	0.05 (0.00)	36.1 (2.4)	394.4 (3.5)	572.5 (5.3)
Ridge (n = 85)	0.14 (0.01)	99.2 (4.0)	436.5 (2.8)	467.2 (4.8)
Willow (n = 175)	0.17 (0.01)	124.1 (7.3)	421.9 (6.5)	456.9 (8.6)
Mean	0.12	88.8	424.0	490.1
Minimum	0.05	36.1	394.4	456.9
Maximum	0.17	124.1	451.3	572.5
Range	0.12	88.0	56.9	115.6

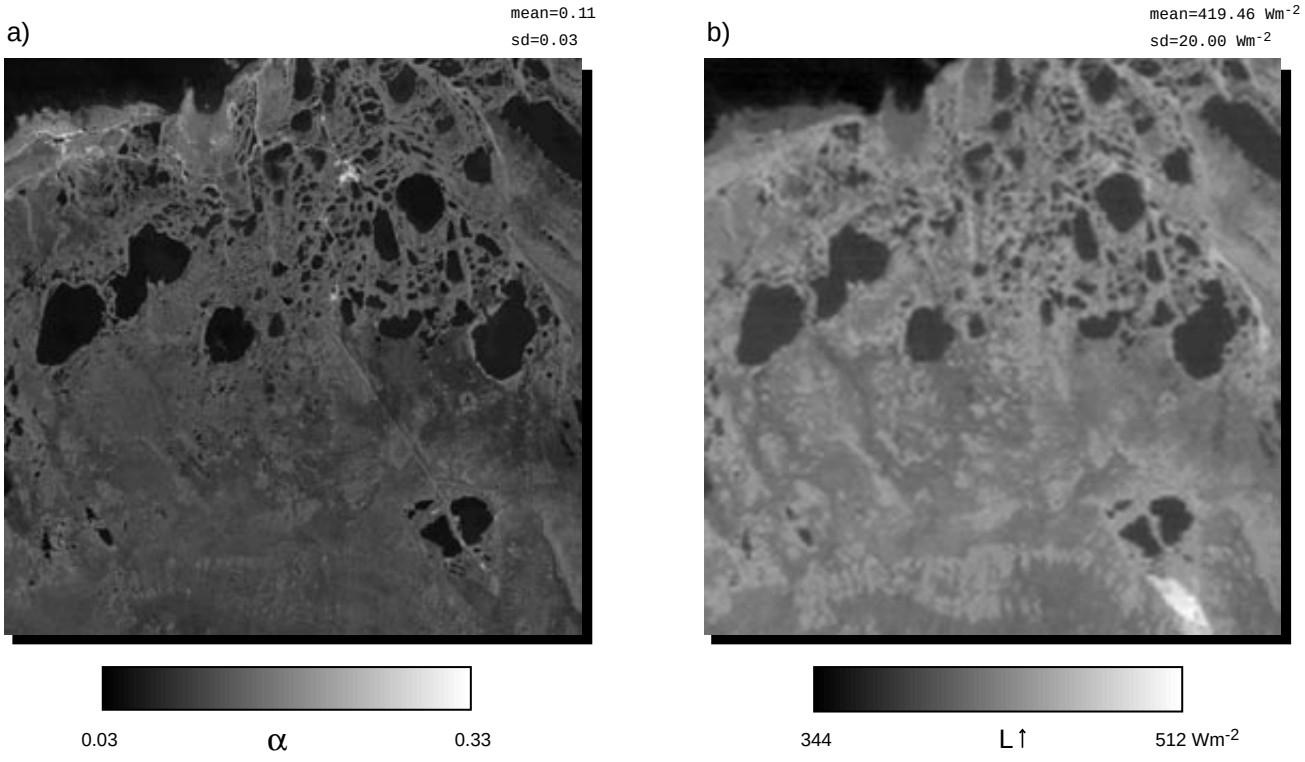

Fig. 5. Example of: (a) surface albedo, (b) surface thermal exitance, and (c) surface net radiation maps derived from Landsat TM data (6 August 1991)

cated earlier, the presence of a complex vegetation canopy (shrubs and trees) masks to some extent changes in surface wetness. However, when all sites are combined, the mean α value from this subarctic tundra-forest landscape on the very wet year (1991) is 0.11 compared to 0.12 for the relatively dry year (1984). Although the maximum difference in mean α for the 5 terrain types is 0.11 (August 1991) to 0.12 (August 1984), both the low variability within terrain types on a given date and the similar mean α in dry and wet years indicate that changes in surface wetness has only a moderate influence on α at the regional scale.

In general, for $L\uparrow$, slightly smaller within terrain type variations are observed in the dryer year (1984). However, under dryer surface conditions, differences between terrain types increase. The sedge site shows the greatest difference between the 2 dates as wetness at this site is tightly linked to the extent of standing water. Q^* also shows smaller within terrain type spatial variability and an increase in difference between terrain types under relatively dry surface conditions.

5. DISCUSSION AND CONCLUSIONS

The results of this study show that components of the surface radiation balance can be derived with reasonable accuracy from Landsat TM data, in most cases to

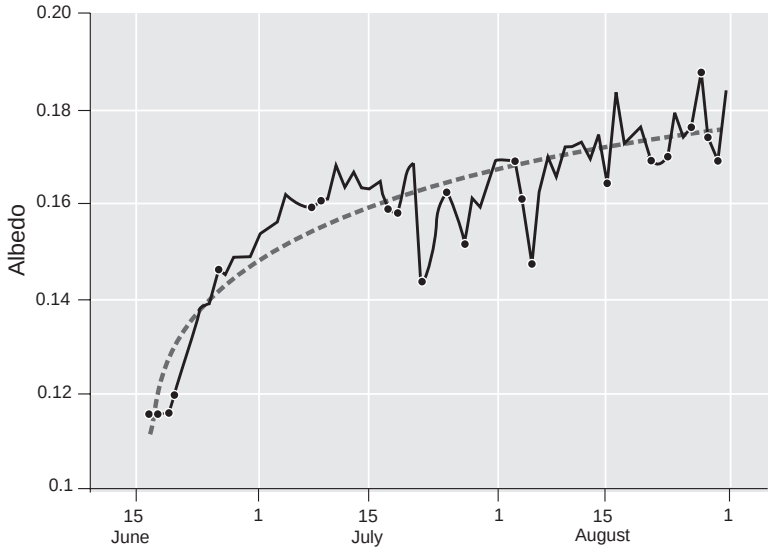

Fig. 6. Seasonal course of mean daily surface albedo at the willow site during summer 1991. Dots mark days with precipitation (from Blanken & Rouse 1994)

within the error of the instruments. α gave the closest agreement between surface and satellite estimates, followed by $L\uparrow$ and Q^*. Mean absolute differences in $K\uparrow$, $L\uparrow$, and Q^* were 6.4 (or α of 0.01), 25.7, and 14.1 W m^{-2}, respectively. Discrepancies between these 2 estimates can be explained in terms of methodology (i.e. contact vs brightness temperatures used to compute $L\uparrow$ and the assumption of a constant emissivity value of 0.98 for all terrain types) and instrument error. We are confident from these results that between terrain differences in the surface radiation balance on the subarctic tundra can be resolved satisfactorily from Landsat TM data.

The Landsat TM data show that within terrain type spatial variation in the surface radiation balance components is greatest for Q^* itself. The largest spatial variations on the 3 dates examined were found at sites with complex vegetation canopies (willow and forest) and the sedge site, for which wetness conditions are strongly influenced by fluctuations of the water table level. Since spatial variation in α (or $K\uparrow$) and $L\uparrow$ was smaller than for Q^* our results suggest that small-scale variations in these fluxes work in concert with one another. Such behaviour is expected if the dominant control is surface wetness, increasing (decreasing) dryness serves to increase (decrease) α and $L\uparrow$ which both translate into a decrease (increase) in Q^* (all other factors being equal).

We feel that there are 3 avenues of research for future studies: (1) satellite calibration, (2) temporal resolution, and (3) spatial scaling issues. Investigation of the Landsat TM calibration coefficients appears to be warranted from this study. Radiances derived from the old and new TM sets of calibration coefficients may have been underestimated. Both calibration sets gave occasional negative radiance values (i.e. radiances lower than path radiances predicted with LOWTRAN 7) over dark targets (e.g. Hudson Bay) in some spectral bands. Spectroradiometric measurements, over the main terrain types found in the Churchill area, will need to be acquired coincident with the satellite overpass in a future investigation. This will permit us to examine more closely the issue of sensor calibration and validation (cal/val) as it relates to Landsat-5 TM or other satellite sensors.

In practical terms the temporal and spatial issues are almost inseparable. Landsat passes give a temporal coverage of every 16 d at best, improvement to every day can be gained by using AVHRR data. However, the spatial resolution of AVHRR (1.1 km) is approximately 30 times less than that of TM imagery (30 m). Our results from simple scaling experiments with the TM data indicate that the scene mean values from the surface radiation balance components were relatively invariant with changes in scale (Fig. 7). However, a larger problem is that small features such as the many ponds in the northern half of the study area are lost at the coarse resolution of AVHRR. It is not clear that similar linear scaling would apply if, for instance, brightness temperature was used to compute fluxes of sensible and latent heat (Fig. 8). Field studies suggest that, because of local advective effects, these small water bodies may play a larger role in the regional water balance than their areal coverage suggests (Bello & Smith 1990, Boudreau & Rouse 1995). For these reasons TM imagery should be compared with AVHRR to investigate the potential for improving the temporal coverage. In addition, methodologies currently being developed for scaling of spectral imagery, such as spectral mixture analysis (Peddle et al. 1999), and the use of semi-variograms (Friedl 1996) need to be tested over the subarctic landscape.

A further temporal scaling issue is the need to move from instantaneous values derived from remote sensing to daily and hourly resolutions. Field data is needed to solve this problem and some approaches have been suggested (Kustas et al. 1994b, Duguay 1995). Full investigation of these methodologies in a range of environments, including the subarctic, is required.

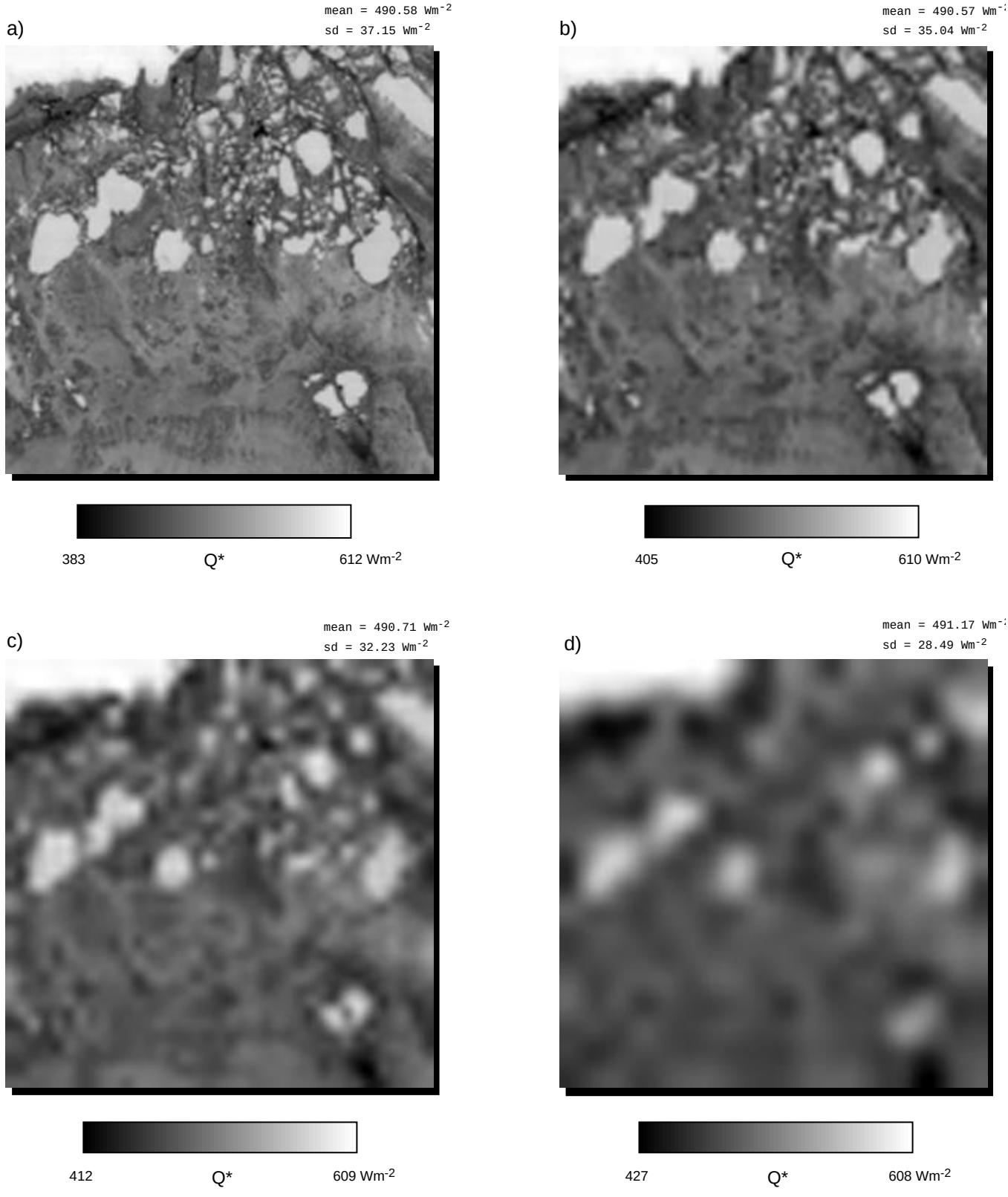

Fig. 7. Surface net radiation map of 6 August 1991 reproduced at: (a) 120 m, (b) 240 m, (c) 480 m, and (d) 960 m pixel resolution, showing the effect of decreasing spatial resolution on regional estimates of the radiation balance. The original 30 m resolution surface net radiation map is shown in Fig. 5c

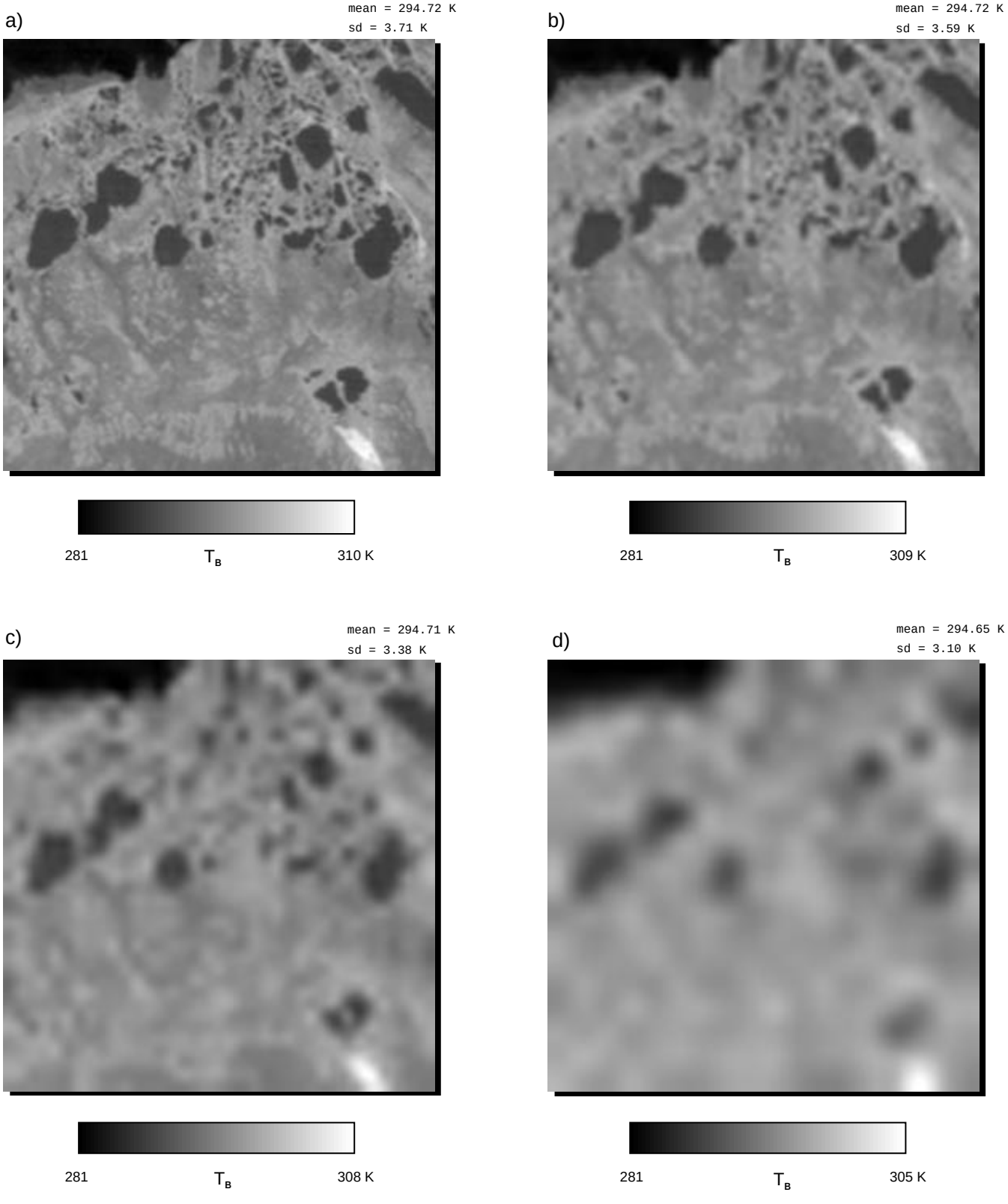

Fig. 8. Surface brightness temperature (T_B) maps of 6 August 1991 reproduced at: (a) 120 m, (b) 240 m, (c) 480 m, and (d) 960 m pixel resolution, showing the effect of decreasing spatial resolution on mean and standard deviation over the study area. Note that many of the small lakes and ponds are lost at the coarser pixel resolution, comparable to that of NOAA AVHRR

Promising solutions for some of these issues will come from new technology. For example, a new array of instruments is planned for the EOS AM-1 platform. To be launched during the third quarter of 1999, this satellite will carry sensors which will allow the mapping of the surface components of the radiation balance at a variety of spatial (15 m to 1.1 km) and temporal (2 to 16 d) resolutions/scales (ASTER, MISR, and MODIS). However, until then, efforts must continue in order to improve current methodologies to estimate these parameters, so that algorithms can be readily applied to the radiances measured by the EOS sensors for operational usage.

In conclusion, the results linking the surface radiation balance, and eventually the surface energy budget, and satellite data are promising. The subarctic landscape of the Hudson Bay Lowlands, while topographically simple, presents several challenges relating to spatial scales. There is a wide variation in surface wetness and in canopy complexity. Some terrain types, such as the smaller ponds which are prevalent toward the coast, are at or below the pixel resolution of the satellites. Much of this region is underlain by permafrost which is undetectable by direct means using remote sensing imagery, but plays an important role in the surface energy balance. Continued remote sensing studies are needed to better understand these important issues.

Acknowledgements. Financial support for this research was provided by the Natural Sciences and Engineering Research Council of Canada (C.R.D., W.R.R., and P.M.L.) and a northern student training grant from the Department of Indian and Northern Affairs (L.D.B.). Logistical support was provided by the Churchill Northern Studies Centre. The authors thank Kathleen Montour and Serge Duchesneau, Université Laval, for their help with the preparation of figures. The thorough and constructive reviews of 3 anonymous reviewers helped to improve the paper.

LITERATURE CITED

Bartolucci LA, Chang M, Anuta P, Graves MR (1988) Atmospheric effects on Landsat TM thermal IR data. IEEE Trans Geosci Remote Sensing 26:171–175

Bello R, Smith J (1990) The effect of weather variability on the energy balance of a lake in the Hudson Bay Lowlands, Canada. Arctic Alpine Res 22:98–107

Blanken PD, Rouse WR (1994) The role of willow-birch forest in the surface energy balance at treeline. Arctic Alpine Res 26:403–411

Boudreau LD, Rouse WR (1995) The role of individual terrain units in the water balance of wetland tundra. Clim Res 5: 31–47

Brest CL (1987) Seasonal albedo of an urban/rural landscape from satellite observations. J Clim Appl Meteorol 26: 1169–1187

Crevier Y, Duguay CR (1993) Estimating the reflectance and albedo of glaciers in the Kluane Range, Yukon Territory, with Landsat TM and digital terrain data. Proceedings of the 16th Canadian Symposium on Remote Sensing, Canadian Remote Sensing Society, Ottawa, p 239–244

Daughtry CST, Kustas WP, Moran MS, Pinter PJ, Jackson RD, Brown RW, Nichols WD, Gay LW (1990) Spectral estimates of net radiation and soil heat flux. Remote Sensing Environ 32:111–124

Duguay CR (1993) Modelling the radiation balance of alpine snow fields with remotely sensed data: model formulation and validation. Ann Glaciol 17:288–294

Duguay CR (1994) Remote sensing of the radiation balance during the growing season at the Niwot Ridge Long-Term Ecological Research site, Front Range, Colorado, U.S.A. Arctic Alpine Res 26:393–402

Duguay CR (1995) An approach to the estimation of surface net radiation in mountain areas using remotely sensed and digital terrain data. Theor Appl Climatol 52:55–68

Duguay CR, LeDrew EF (1991) Mapping surface albedo in the east slope of the Colorado Front Range, U.S.A., with Landsat Thematic Mapper. Arctic Alpine Res 23:213–223

Duguay CR, LeDrew EF (1992) Estimating surface reflectance and albedo from Landsat-5 Thematic Mapper over rugged terrain. Photogram Eng Remote Sensing 58:551–558

Friedl MA (1996) Relationships among remotely sensed data, surface energy balance, and area-averaged fluxes over partially vegetated land surfaces. J Appl Meteorol 35: 2091–2103

Humes KS, Kustas WP, Moran MS, Nichols WD, Weltz MA (1994) Variability of emissivity and surface temperature over a sparsely vegetated surface. Water Resour Res 30: 1299–1310

Knap WH (1997) Satellite-derived and ground-based measurements of the surface albedo of glaciers. PhD thesis, Utrecht University

Koelemeijer R, Oerlemans J, Tjemkes S (1993) Surface reflectance of Hintereisferner, Austria, from Landsat 5 TM imagery. Ann Glaciol 17:17–22

Kustas WP, Moran MS, Jackson RD, Gay LW, Duell LFW, Kunkel KE, Matthias AD (1990) Instantaneous and daily values of the surface energy balance over agricultural fields using remote sensing and a reference field in an arid environment. Remote Sensing Environ 32:125–141

Kustas WP, Moran MS, Humes KS, Stannard DI, Pinter PJ, Hipps LE, Swiatek E, Goodrich DC (1994a) Surface energy balance estimates at local and regional scales using optical remote sensing from an aircraft platform and atmospheric data collected over semiarid rangelands. Water Resour Res 30:141–1259

Kustas WP, Pinker RT, Schmugge TJ, Humes KS (1994b) Daytime net radiation estimated for a semiarid rangeland basin from remotely sensed data. Agric For Meteorol 71: 337–357

Lafleur PM, Renzetti AV, Bello R (1993) Seasonal changes in the radiation balance of subarctic forest and tundra. Arctic Alpine Res 25:32–36

Lafleur PM, Wurtele AB, Duguay CR (1997) Spatial and temporal variations in surface albedo of a subarctic landscape using surface-based measurements and remote sensing. Arctic Alpine Res 29:261–269

Lathrop RG, Lillesand TM (1987) Calibration of Thematic Mapper data for water surface temperature mapping: case study on the Great Lakes. Remote Sensing Environ 22: 297–307

Moran MS, Clarke TR, Kustas WP, Weltz M, Amer SA (1994) Evaluation of hydrologic parameters in a semiarid rangeland using remotely sensed spectral data. Water Resour Res 30:1287–1297

Moran MS, Jackson RD, Clarke TR, Qi J, Cabot F, Thome KJ, Markham BL (1995) Reflectance factor retrieval from Landsat TM and SPOT HRV for bright and dark targets. Remote Sensing Environ 52:218–230

Peddle DR, Hall FG, LeDrew EF (1999) Spectral mixture analysis and geometric-optical reflectance modeling of boreal forest biophysical structure. Remote Sensing Environ 67:288–297

Pierce LL, Congalton RG (1988) A methodology for mapping forest latent heat flux densities using remote sensing. Remote Sensing Environ 24:405–418

Rouse WR (1984) Microclimate at Arctic treeline: I. Radiation balance of tundra and forest. Water Resour Res 20:57–66

Schott JR, Volchok WJ (1985) Thematic Mapper thermal infrared calibration. Photogram Eng Remote Sensing 51:1351–1357

Teillet PM, Fedosejevs G (1995) On the dark target approach to atmospheric correction of remotely sensed data. Can J Remote Sensing 21:374–387

Wukelic GE, Gibbons DE, Martucci LM, Foote HP (1989) Radiometric calibration of Landsat Thematic Mapper thermal band. Remote Sensing Environ 28:339–347

Editorial responsibility: Lawrence Kalkstein, Newark, Delaware, USA

Submitted: May 8, 1997; Accepted: May 16, 1999
Proofs received from author(s): July 12, 1999